energies

MDPI

Article

Immersion and Invariance Adaptive Backstepping Control of PEMFC Air Supply Systems with Unmeasurable Cathode Air Pressure

Qi Han [1,2], Xinfeng Zhang [1,*], Shusheng Xiong [2], Zhitao Liu [3] and Mingyong Fu [4]

[1] School of Information and Electrical Engineering, Hangzhou City University, Hangzhou 310015, China; qhan@hzcu.edu.cn
[2] College of Energy Engineering, Zhejiang University, Hangzhou 310012, China; xiongss@zju.edu.cn
[3] Institute of Cyber-Systems and Control, Zhejiang University, Hangzhou 310012, China; ztliu@zju.edu.cn
[4] Beijing Zhuoyi Intelligent Technology Co., Ltd., Beijing 100088, China; fmy198377@126.com
* Correspondence: zxf@hzcu.edu.cn

Abstract

In this paper, an immersion and invariance (I&I) adaptive backstepping control strategy is proposed for proton exchange membrane fuel cell (PEMFC) air supply systems with unmeasurable cathode air pressure. To account for uncertainties such as gas leakage and stack temperature variation, an I&I adaptive full-state feedback control strategy is first proposed, which ensures asymptotic regulation of the oxygen excess ratio (OER) while maintaining satisfactory transient performance. Since the cathode air pressure is not directly accessible via sensor measurements, state reconstruction based on available output data becomes a necessity. To address this issue, an I&I adaptive observer-based partial-state feedback control strategy is then proposed, where the unknown parameters and the unmeasurable state are treated in a uniform manner. The stability of the closed-loop system is established via Lyapunov analysis, and the efficacy of the proposed control schemes is validated through numerical simulations under parametric variations.

Keywords: adaptive observer; backstepping control; immersion and invariance; parametric uncertainty; proton exchange membrane fuel cell (PEMFC)

1. Introduction

Fuel cell systems represent a clean method for energy production and are currently the subject of extensive development efforts. Proton exchange membrane fuel cells (PEMFCs) are characterized by several advantageous attributes, including high power density, fast startup capability, low noise, and environmental compatibility [1–5]. Consequently, they have found extensive application in diverse sectors such as laptops, hybrid vehicles and power generation [6,7], to mention a few.

A PEMFC constitutes a complex, multi-physics system comprising several interconnected subsystems. The four main subsystems in a PEMFC can be decoupled by adopting a time-scale argument, in which the dynamic behavior of the air supply subsystem is described by a highly uncertain nonlinear model [8]. The oxygen excess ratio (OER) constitutes a key metric for evaluating the performance of the air supply subsystem, which quantifies the ratio between the oxygen inflow delivered to the cathode and the oxygen consumed during the electrochemical conversion process. Precise regulation of the OER is therefore essential but also challenging to prevent oxygen starvation during load transients, necessitating advanced control schemes.

Check for updates

Academic Editors: Gabriele Discepoli and JongHoon Kim

Received: 8 September 2026
Revised: 16 October 2026
Accepted: 20 October 2026
Published: 27 October 2026

Copyright: © 2026 by the authors. Licensee MDPI, Basel, Switzerland. This article is an open access article distributed under the terms and conditions of the Creative Commons Attribution (CC BY) license.

Classical feedback and feed-forward control employing proportional–integral–derivative (PID) controllers represents the most prevalent control methodology for enhancing fuel cell performance [1], however, the nonlinear and complex dynamics of PEMFC systems associated with fuel starvation necessitate control strategies capable of responding more rapidly and with greater precision. In response, advanced nonlinear control paradigms have emerged as promising alternatives to classical architectures. To enhance the robustness of the closed-loop system, sliding mode control (SMC) methods have been introduced in the literature [9–12]. These approaches are capable of handling nonlinearities and uncertainties without imposing a heavy computational burden on the controller algorithm, owing to the incorporation of a switching robust term. To compensate for uncertainties inherent in air supply systems, adaptive control techniques have been widely favored in the literature. Through parameter identification and pole assignment, Ref. [13] proposes an adaptive controller to dynamically stabilize the OER around an optimal level. Utilizing backstepping technique and neural network, an adaptive controller is proposed in [14] for OER regulation in presence of modeling errors, external disturbances and uncertainties. To accommodate unknown air compressor faults, Ref. [15] proposes an adaptive prescribed performance controller for OER using a bound estimation approach, and [16] utilizes an estimator-based adaption law to ensure reliable OER regulation under multiple fault occurrences. For coordinated regulation of air flow rate and cathode pressure, an adaptive backstepping controller is proposed in [17] which allows all model parameters to be uncertain. Moreover, a distributed deep reinforcement learning-based adaptive proportional integral controller is developed in [18] for controlling air flow. Furthermore, to enhance control performance, robust and adaptive control techniques are often integrated [19–21], giving rise to more advanced schemes capable of delivering both accuracy and robustness.

Most adaptive schemes developed for the air supply system of a PEMFC rely on Lyapunov-based adaptive control, which follows the design principle of canceling out the known terms multiplying to the parameter estimation error in the time-derivative of a suitable composite Lyapunov function. Departure from it, immersion and invariance (I&I) adaptive control [22] does not cancel out the estimation error-related terms but dominate them via introducing an auxiliary function to the estimate. An important advantage of this method is that it outperforms classical Lyapunov-based adaptive method in term of transient performance. On the other hand, many existing robust or adaptive control methods rely on full-state feedback. However, owing to mechanical constraints and the prohibitive cost of sensing technology [10,23], direct measurement of all system states is not always feasible. Consequently, certain states may remain unmeasured, posing a challenge for control design. Among existing approaches, model-based observer techniques are widely adopted to reconstruct unknown states, see, e.g., [24] for a detailed review. Notably, extended state observers (ESOs) have gained particular traction in this context, as they offer the capability to recover unmeasured states while simultaneously estimating external disturbances and capturing the underlying plant dynamics [10,16,21,25]. While ESOs are effective in state reconstruction, existing analyses tend to treat observation error dynamics and output error dynamics separately. This observation provides the motivation for the unified adaptive observer framework developed herein.

In this paper, an I&I adaptive control framework is proposed for the air supply system of a PEMFC subject to unmeasurable states. An I&I adaptive full-state feedback controller is first designed to achieve asymptotic OER regulation in the presence of parametric uncertainties. To address the practical limitation that cathode air pressure cannot be directly measured, an I&I adaptive observer-based partial-state feedback strategy is subsequently developed, treating unknown parameters and unmeasured states within a unified estimation framework. Closed-loop stability is proven via Lyapunov methods. Numerical

tests covering plant parameter variations, initial parameter estimation errors and process disturbances are conducted, and quantitative indices are adopted to assess both regulation and state reconstruction performance.

The main contributions of this paper are as follows. (1) The proposed full-state feedback I&I adaptive controller, tailored for the nonlinear PEMFC air supply dynamics, achieves asymptotic OER regulation and yields improved transient performance compared with conventional Lyapunov-based adaptive schemes, with rigorous stability analysis for the closed-loop regulation error. (2) A novel I&I adaptive observer is developed for the partial-state feedback architecture. It simultaneously performs parameter adaptation and state reconstruction to guarantee asymptotic convergence of the observation error. The unmeasurable cathode pressure is recovered by the observer, which removes the requirement for an extra in-channel cathode pressure sensor. (3) A unified adaptive observer-controller framework is proposed for OER regulation with asymptotic convergence. Unlike ESO-based alternatives, where state observation and feedback control are designed in a decoupled fashion [10,16,21,25], the proposed I&I approach integrates the observer and control law within a single stability framework.

The remainder of this paper is organized as follows. Section 2 presents the dynamic modeling of the PEMFC air supply system and formulates the OER regulation problem. In Section 3, an I&I adaptive full-state feedback control strategy is first developed. Section 4 extends this framework by proposing an I&I adaptive observer-based partial-state feedback control strategy. Finally, Section 5 carries out simulated results and Section 6 concludes the paper.

2. System Modeling and Problem Formulation

Consider the following third-order nonlinear model of PEMFC air supply system [8]:

$$\begin{aligned} \dot{x}_1 &= -\mu_1 x_1 + \mu_2 x_3 + \mu_3 - \mu_4 I_{st} \\ \dot{x}_2 &= -c_9 x_2 - \frac{c_{10}}{x_2}\varphi(x_3)h(x_2, x_3) + c_{13}u \\ \dot{x}_3 &= \phi(x_3)[h(x_2, x_3) + c_{16}(x_1 - x_3)] \end{aligned} \tag{1}$$

where $x_1 \in \mathbb{R}_+$ is the air pressure in the cathode, $x_2 \in \mathbb{R}_+$ is the angular speed of the compressor, $x_3 \in \mathbb{R}_+$ is the supply manifold pressure, $I_{st} \in \mathbb{R}_+$ is the measurable load current, $u \in \mathbb{R}_+$ is the compressor motor voltage which is viewed as the control input, and $h(x_2, x_3) \in \mathbb{R}$ is the air mass flow variable, whose explicit expression can be found in [16,26]. The functions $\varphi(x_3)$ and $\phi(x_3)$ are given by $\varphi(x_3) = \left(\frac{x_3}{c_{11}}\right)^{c_{12}} - 1$ and $\phi(x_3) = c_{13}[1 + c_{14}\varphi(x_3)]$, and the physical parameters $c_i \in \mathbb{R}_+$ and $\mu_i \in \mathbb{R}_+$ with their units and values can be referred to [27].

To prevent oxygen starvation and sustain peak net power output, the OER λ_{O_2} should be maintained at an optimal reference value of $\lambda_{O_2,ref} = 2$, even under varying load current conditions. Hence, the system output to be regulated is defined as

$$y = \lambda_{O_2} = \frac{W_{O_2,in}}{W_{O_2,react}} = \frac{c_{23}(x_3 - x_1)}{c_{24} I_{st}} \tag{2}$$

where $W_{O_2,in}$ denotes the oxygen inflow to the cathode of the PEMFC system, and $W_{O_2,react}$ is the amount consumed in the reaction.

The objective of this paper is to design a dynamic full/partial-state feedback controller for (1) such that all closed-loop signals are bounded, and

$$\lim_{t\to\infty} y(t) - y_r = 0 \tag{3}$$

where $y_r = \lambda_{O_2,ref}$.

Remark 1. *In this paper, we focus on the uncertainties associated with parameters $\mu_1, \cdots, \mu_4$ and c_9. These uncertainties arise in practice due to the following factors, as pointed out by numerous research works. Specifically, the cathode volume may have uncertain changes due to gas leakage or blockage, and the stack temperature is influenced by the cooling system regulation and gas flow rates [17], leading to uncertainties in $\mu_1, \cdots, \mu_4$. Moreover, leaking and faults in the air supply system have an impact on compressor motor parameter in c_9 [15,16].*

Remark 2. *In addition to full-state feedback, the case of unmeasurable cathode pressure x_1 is also investigated in this paper as in [10,16,21,25]. Since the OER depends explicitly on this unmeasured state, the regulation objective itself becomes unavailable for direct feedback, introducing a sophisticated control challenge. In response to this challenge, an I&I adaptive observer is proposed in Section 4, which is specifically designed to achieve asymptotic convergence of the observation error.*

The following assumption with regard to the load current I_{st} is made, similar to that introduced in [28].

Assumption 1. *The load current I_{st} and its derivatives $\dot{I}_{st}$ and $\ddot{I}_{st}$ are measurable, and I_{st}, $\dot{I}_{st}$ and $\ddot{I}_{st}$ are all bounded.*

Remark 3. *Note that the load current may be assumed constant to simplify analysis, owing to the separation of time scales between electrical and mechanical dynamics [23]. In this work, nevertheless, the stability analysis is extended to the time-varying load case to accommodate more general operating scenarios.*

3. Full-State Feedback Control

In this section, a full-state feedback controller based on I&I estimator for (1) is proposed. I&I estimators are designed to estimate the unknown parameters, and then the control law based on backstepping is constructed to stabilize the OER error.

3.1. I&I Estimator Design

Denote $\theta_1 := [\mu_1, \mu_2, \mu_3, \mu_4]^T$, $\Phi_1(x_1, x_3, I_{st}) := [-x_1, x_3, 1, -I_{st}]^T$, $\theta_2 := c_9$ and $\bar{u} := c_{13}u - \frac{c_{10}}{x_2}\varphi(x_3)h(x_2, x_3)$; rewrite (x_1, x_2)-dynamics in (1) as

$$\begin{aligned} \dot{x}_1 &= \theta_1^T \Phi_1 \\ \dot{x}_2 &= -\theta_2 x_2 + \bar{u} \end{aligned} \tag{4}$$

where the abbreviation $\Phi_1 := \Phi_1(x_1, x_3, I_{st})$ is used. The I&I estimates are updated by

$$\begin{aligned} \dot{\hat{\theta}}_1 &= -\frac{\partial \beta_1}{\partial x_1}(\hat{\theta}_1 + \beta_1)^T \Phi_1 - \frac{\partial \beta_1}{\partial x_3}\dot{x}_3 - \frac{\partial \beta_1}{\partial I_{st}}\dot{I}_{st} \\ \frac{\partial \beta_1}{\partial x_1} &= \gamma_1 \Phi_1 \\ \dot{\hat{\theta}}_2 &= -\frac{\partial \beta_2}{\partial x_2}[-(\hat{\theta}_2 + \beta_2)x_2 + \bar{u}] \\ \frac{\partial \beta_2}{\partial x_2} &= -\gamma_2 x_2 \end{aligned} \tag{5}$$

with $\gamma_1 \in \mathbb{R}^{4\times 4} > 0$ being the diagonal adaptation gain matrix and $\gamma_2 > 0$. The time-derivatives of the estimation errors $\tilde{\theta}_1 := \hat{\theta}_1 + \beta_1 - \theta_1$ and $\tilde{\theta}_2 := \hat{\theta}_2 + \beta_2 - \theta_2$ are

$$\begin{aligned} \dot{\tilde{\theta}}_1 &= -\gamma_1 \Phi_1 \Phi_1^T \tilde{\theta}_1 \\ \dot{\tilde{\theta}}_2 &= -\gamma_2 x_2^2 \tilde{\theta}_2. \end{aligned} \tag{6}$$

Consider the following composite function,

$$V_{\tilde{\theta}} = \frac{1}{2}\tilde{\theta}_1^T\gamma_1^{-1}\tilde{\theta}_1 + \frac{1}{2\gamma_2}\tilde{\theta}_2^2 \tag{7}$$

whose time derivative satisfies

$$\dot{V}_{\tilde{\theta}} = -(\Phi_1^T\tilde{\theta}_1)^2 - x_2^2\tilde{\theta}_2^2 \leq 0 \tag{8}$$

which implies that $\tilde{\theta}_1(t)$ and $\tilde{\theta}_2(t)$ are bounded.

Remark 4. *According to (5), the auxiliary functions β_1, β_2 can be chosen as*

$$\beta_1(x_1, x_3, I_{st}) = \gamma_1\left[-\frac{x_1^2}{2}, x_3x_1, x_1, -I_{st}x_1\right]^T$$
$$\beta_2(x_2) = -\gamma_2\frac{x_2^2}{2}.$$

3.2. Backstepping Control Design

Define the following compensated error variables

$$z_1 := y - y_r, \quad z_2 := \Xi(x_2, x_3, I_{st}) - \alpha \tag{9}$$

where $\Xi(x_2, x_3, I_{st}) := m(I_{st})\phi(x_3)h(x_2, x_3)$ with $m := \frac{c_{23}}{c_{24}I_{st}}$, and α is the virtual control law to be designed, whose arguments will be specified in the subsequent development. The control design will be presented in the following two steps.

Step 1. The time derivative of z_1 is

$$\begin{aligned}\dot{z}_1 &= m(\dot{x}_3 - \dot{x}_1) + \dot{m}(x_3 - x_1)\\ &= \Xi + mc_{16}\phi(x_1 - x_3) - m\theta_1^T\Phi_1 + \dot{m}(x_3 - x_1)\\ &= z_2 + \alpha + f_1 - m\theta_1^T\Phi_1\end{aligned} \tag{10}$$

with $f_1 := mc_{16}\phi(x_1 - x_3) + \dot{m}(x_3 - x_1)$ where $\dot{m} = -\frac{c_{23}\dot{I}_{st}}{c_{24}I_{st}^2}$. Design the virtual control α as

$$\alpha = -(k_1 + m^2\epsilon)z_1 + m(\hat{\theta}_1 + \beta_1)^T\Phi_1 - f_1 \tag{11}$$

with $\epsilon > 0$, which yields

$$\dot{z}_1 = -(k_1 + m^2\epsilon)z_1 + z_2 + m\tilde{\theta}_1^T\Phi_1. \tag{12}$$

Step 2. To proceed, compute the time-derivative of z_2 as

$$\begin{aligned}\dot{z}_2 &= \frac{\partial\Xi}{\partial x_2}(-\theta_2x_2 + \bar{u}) + \frac{\partial\Xi}{\partial x_3}\dot{x}_3 + \frac{\partial\Xi}{\partial I_{st}}\dot{I}_{st} - \dot{\alpha}\\ &= g(-\theta_2x_2 + \bar{u}) + \frac{\partial\Xi}{\partial x_3}\dot{x}_3 + \frac{\partial\Xi}{\partial I_{st}}\dot{I}_{st} - \frac{\partial\alpha}{\partial x_1}(\hat{\theta}_1 + \beta_1 - \tilde{\theta}_1)^T\Phi_1 - \frac{\partial\alpha}{\partial x_3}\dot{x}_3 - \frac{\partial\alpha}{\partial\hat{\theta}_1}\dot{\hat{\theta}}_1\\ &\quad - \frac{\partial\alpha}{\partial I_{st}}\dot{I}_{st} - \frac{\partial\alpha}{\partial\dot{I}_{st}}\ddot{I}_{st}\\ &= g(-\theta_2x_2 + \bar{u}) + f_2 + \frac{\partial\alpha}{\partial x_1}\tilde{\theta}_1^T\Phi_1\end{aligned} \tag{13}$$

where $g := \frac{\partial\Xi}{\partial x_2}$ and $f_2 := \frac{\partial\Xi}{\partial x_3}\dot{x}_3 - \frac{\partial\alpha}{\partial x_1}\left(\hat{\theta}_1 + \beta_1\right)^T\Phi_1 - \frac{\partial\alpha}{\partial x_3}\dot{x}_3 - \frac{\partial\alpha}{\partial\hat{\theta}_1}\dot{\hat{\theta}}_1 + \frac{\partial\Xi}{\partial I_{st}}\dot{I}_{st} - \frac{\partial\alpha}{\partial I_{st}}\dot{I}_{st} - \frac{\partial\alpha}{\partial\dot{I}_{st}}\ddot{I}_{st}$. Note that $g > 0$ as indicated in [23,27]; hence, the control law to be designed is well-defined. Design the control law u as

$$\begin{aligned}\bar{u} &= \frac{1}{g}\left[-z_1 - k_2z_2 - \frac{\epsilon}{2}\left(\frac{\partial\alpha}{\partial x_1}\right)^2z_2 - \frac{\epsilon}{2}g^2z_2 + (\hat{\theta}_2 + \beta_2)gx_2 - f_2\right]\\ u &= \frac{1}{c_{13}}\left(\bar{u} + \frac{c_{10}}{x_2}\varphi h\right).\end{aligned} \tag{14}$$

Substituting $\bar{u}$ into $\dot{z}_2$ yields

$$\dot{z}_2 = -z_1 - k_2 z_2 - \frac{\epsilon}{2}\left(\frac{\partial \alpha}{\partial x_1}\right)^2 z_2 - \frac{\epsilon}{2} g^2 z_2 + \frac{\partial \alpha}{\partial x_1}\tilde{\theta}_1^T \Phi_1 + \tilde{\theta}_2 g x_2 \tag{15}$$

Now consider the following function,

$$V_z = \frac{1}{2} z_1^2 + \frac{1}{2} z_2^2 \tag{16}$$

whose time derivative satisfies

$$\dot{V}_z = -(k_1 + m^2\epsilon) z_1^2 + m z_1 \tilde{\theta}_1^T \Phi_1 - k_2 z_2^2 - \frac{\epsilon}{2}\left(\frac{\partial \alpha}{\partial x_1}\right)^2 z_2^2 - \frac{\epsilon}{2} g^2 z_2^2 + \frac{\partial \alpha}{\partial x_1}\tilde{\theta}_1^T \Phi_1 z_2 + \tilde{\theta}_2 g z_2 x_2. \tag{17}$$

Using the inequalities $m z_1 \tilde{\theta}_1^T \Phi_1 \leq \frac{1}{4\epsilon}\left(\tilde{\theta}_1^T \Phi_1\right)^2 + m^2 \epsilon z_1^2$, $\frac{\partial \alpha}{\partial x_1}\tilde{\theta}_1^T \Phi_1 z_2 \leq \frac{1}{2\epsilon}\left(\tilde{\theta}_1^T \Phi_1\right)^2 + \frac{\epsilon}{2}\left(\frac{\partial \alpha}{\partial x_1}\right)^2 z_2^2$ and $\tilde{\theta}_2 g z_2 x_2 \leq \frac{1}{2\epsilon}\tilde{\theta}_2^2 x_2^2 + \frac{\epsilon}{2} g^2 z_2^2$, then

$$\dot{V}_z \leq -k_1 z_1^2 - k_2 z_2^2 + \frac{3}{4\epsilon}(\tilde{\theta}_1^T \Phi_1)^2 + \frac{1}{2\epsilon}\tilde{\theta}_2^2 x_2^2. \tag{18}$$

3.3. Stability Analysis for the Full-State Feedback Case

The stability analysis of the closed-loop system for the full-state feedback case is presented in the following theorem.

Theorem 1. *For system (1), it is closed with the adaptive law (5) and the control laws (11) and (14). Under Assumption 1, it can be guaranteed that all closed-loop signals are bounded and the output error $z_1(t)$ converges to zero as time goes infinity.*

Proof. Choose the following function

$$V_1 = \frac{1}{\epsilon} V_{\tilde{\theta}} + V_z \tag{19}$$

whose derivative satisfies, in view of (8) and (18),

$$\dot{V}_1 \leq -k_1 z_1^2 - k_2 z_2^2 - \frac{1}{4\epsilon}(\tilde{\theta}_1^T \Phi_1)^2 - \frac{1}{2\epsilon}\tilde{\theta}_2^2 x_2^2 \leq 0 \tag{20}$$

from which we know $V_1(t)$ is bounded and so are $z_1(t)$ and $z_2(t)$. The boundedness of $z_1(t)$ gives the boundedness of y. From [2] we know x_1 is bounded with a bounded y. As a result, all closed-loop signals are bounded. Furthermore, integrate both sides of (20) yields

$$\begin{aligned} V_1(\infty) \leq & -k_1 \int_0^\infty z_1(\zeta)^2 d\zeta - k_2 \int_0^\infty z_2(\zeta)^2 d\zeta \\ & - \frac{1}{4\epsilon}\int_0^\infty (\Phi_1(\zeta)^T \tilde{\theta}_1(\zeta))^2 d\zeta \\ & - \frac{1}{2\epsilon}\int_0^\infty (x_2(\zeta)\tilde{\theta}_2(\zeta))^2 d\zeta + V_1(0). \end{aligned}$$

By invoking standard analysis procedure using Barbalat's lemma we can derive that $\lim_{t\to\infty} z_1(t) = 0$. This completes the proof. □

Remark 5. *From the above analysis, it can be observed that the cross terms $\Phi_1(t)^T \tilde{\theta}_1(t)$ and $x_2(t)\tilde{\theta}_2(t)$ with respect to estimation error is square integrable. Notably, this property is not generally guaranteed by traditional Lyapunov-based adaptive methods. Consequently, the proposed control scheme is capable of enhancing the transient performance of OER regulation. While the proposed method guarantees boundedness of parameter estimation errors and asymptotic OER regulation, but exact convergence of estimated parameters to their true values is not guaranteed in the absence of the persistent-excitation condition.*

4. Partial-State Feedback Control Using an I&I Adaptive Observer

Due to mechanical constraints and the prohibitive cost of sensing technology, the cathode air pressure x_1 may not be available for feedback. In this section, we consider the design of the partial-state feedback controller by further utilizing I&I theory. Different from decoupled ESO-based strategies where the observer and control law are designed independently, the proposed I&I scheme integrates parameter adaptation and state reconstruction into one unified framework. This feature enables asymptotic convergence for both state observation error and OER regulation error within a unified theoretical framework.

Since x_1 is unavailable, then the original output y can not be used. Define the following error variables, analogous to (9):

$$z_1 := \hat{y} - y_r, \quad z_2 := \Xi(x_2, x_3, I_{st}) - \alpha \tag{21}$$

where variable $\hat{y}$ to be regulated is defined as

$$\hat{y} = \frac{c_{23}[x_3 - (\hat{x}_1 + \beta_{x_1}(x_3))]}{c_{24} I_{st}} \tag{22}$$

where $\hat{x}_1 + \beta_{\hat{x}_1}(x_3)$ is the I&I observer for the state x_1 with the auxiliary function $\beta_{\hat{x}_1}(x_3)$ to be determined.

4.1. I&I Adaptive Observer Design

Rewrite (x_1, x_3)-dynamics in (1) as

$$\begin{aligned} \dot{x}_1 &= \theta_1^T \Phi_1(x_1, x_3, I_{st}) \\ \dot{x}_3 &= \xi_2(x_2, x_3) + \xi_1(x_3) x_1 \end{aligned} \tag{23}$$

with $\xi_1(x_3) = c_{16}\phi(x_3)$ and $\xi_2(x_2, x_3) := \phi(x_3)h(x_2, x_3) - \xi_1 x_3$. Define the observation error $\tilde{x}_1 := \hat{x}_1 + \beta_{\hat{x}_1}(x_3) - x_1$. Rewrite the above as

$$\begin{aligned} \dot{x}_1 &= \theta_1^T \hat{\Phi}_1 + \mu_1 \tilde{x}_1 \\ \dot{x}_3 &= \xi_2 + \xi_1(\hat{x}_1 + \beta_{\hat{x}_1} - \tilde{x}_1) \end{aligned} \tag{24}$$

where $\hat{\Phi}_1 := \Phi_1(\hat{x}_1 + \beta_{\hat{x}_1}, x_3, I_{st})$ has been defined for abbreviation. At this stage, design the I&I adaptive observer as

$$\begin{aligned} \dot{\hat{x}}_1 &= -\frac{\partial \beta_{\hat{x}_1}}{\partial x_3}[\xi_2 + \xi_1(\hat{x}_1 + \beta_{\hat{x}_1})] + (\hat{\theta}_1 + \beta_1)^T \hat{\Phi}_1 \\ \frac{\partial \beta_{\hat{x}_1}}{\partial x_3} &= \Gamma_1 \\ \dot{\hat{\theta}}_1 &= -\frac{\partial \beta_1}{\partial x_3}[\xi_2 + \xi_1(\hat{x}_1 + \beta_{\hat{x}_1})] - \frac{\partial \beta_1}{\partial \hat{x}_1}\dot{\hat{x}}_1 - \frac{\partial \beta_1}{\partial I_{st}}\dot{I}_{st} \\ \frac{\partial \beta_1}{\partial x_3} &= \gamma_1 \frac{\hat{\Phi}_1}{\xi_1} \end{aligned} \tag{25}$$

with γ_1 defined the same as in the previous section and $\Gamma_1 > 0$. Note that, as pointed out in [23,27], the function $\xi_1 > 0$ for all $x_3 \in \mathbb{R}_+$, and the partial derivative $\frac{\partial \beta_1}{\partial x_3}$ above is well-defined. The time-derivative of $\tilde{x}_1$ is calculated as

$$\begin{aligned} \dot{\tilde{x}}_1 &= \dot{\hat{x}}_1 + \frac{\partial \beta_{\hat{x}_1}}{\partial x_3}[\xi_2 + \xi_1(\hat{x}_1 + \beta_{\hat{x}_1} - \tilde{x}_1)] \\ &\quad - (\hat{\theta}_1 + \beta_1 - \tilde{\theta}_1)^T \hat{\Phi}_1 - \mu_1 \tilde{x}_1 \\ &= -\Gamma_1 \xi_1 \tilde{x}_1 + \tilde{\theta}_1^T \hat{\Phi}_1 - \mu_1 \tilde{x}_1. \end{aligned} \tag{26}$$

On the other hand, the time-derivative of $\tilde{\theta}_1$ is calculated as

$$\begin{aligned}\dot{\tilde{\theta}}_1 &= \dot{\hat{\theta}}_1 + \frac{\partial \beta_1}{\partial x_3}[\xi_2 + \xi_1(\hat{x}_1 + \beta_{\hat{x}_1} - \tilde{x}_1)] + \frac{\partial \beta_1}{\partial \hat{x}_1}\dot{\hat{x}}_1 + \frac{\partial \beta_1}{\partial I_{st}}\dot{I}_{st} \\ &= -\gamma_1 \hat{\Phi}_1 \tilde{x}_1.\end{aligned} \tag{27}$$

Consider the following composite function,

$$V_{(\tilde{x}_1,\tilde{\theta}_1)} = \frac{1}{2}\tilde{\theta}_1^T \gamma_1^{-1}\tilde{\theta}_1 + \frac{1}{2}\tilde{x}_1^2 \tag{28}$$

whose time derivative satisfies

$$\begin{aligned}\dot{V}_{(\tilde{x}_1,\tilde{\theta}_1)} &= -\Gamma_1\xi_1\tilde{x}_1^2 + \tilde{x}_1\tilde{\theta}_1^T\hat{\Phi}_1 - \mu_1\tilde{x}_1^2 - \tilde{\theta}_1^T\hat{\Phi}_1\tilde{x}_1 \\ &= -\Gamma_1\xi_1\tilde{x}_1^2 - \mu_1\tilde{x}_1^2.\end{aligned} \tag{29}$$

4.2. Control Law Synthesis

Step 1. Calculate the time derivative of z_1 as

$$\begin{aligned}\dot{z}_1 &= m[\dot{x}_3 - (\dot{\hat{x}}_1 + \dot{\beta}_{x_1})] + \dot{m}[x_3 - (\hat{x}_1 + \beta_{x_1})] \\ &= z_2 + \alpha + m\xi_1(\hat{x}_1 + \beta_{\hat{x}_1} - \tilde{x}_1 - x_3) \\ &\quad + m\Gamma_1\xi_1\tilde{x}_1 - m(\hat{\theta}_1 + \beta_1)^T\hat{\Phi}_1 + \dot{m}[x_3 - (\hat{x}_1 + \beta_{x_1})] \\ &= z_2 + \alpha + f_3 + \varpi_1\tilde{x}_1 - m(\hat{\theta}_1 + \beta_1)^T\hat{\Phi}_1\end{aligned} \tag{30}$$

with $f_3 = m\xi_1(\hat{x}_1 + \beta_{\hat{x}_1} - x_3) + \dot{m}[x_3 - (\hat{x}_1 + \beta_{x_1})]$ and $\varpi_1 = m(\Gamma_1\xi_1 - \xi_1)$. Design the virtual control α as

$$\alpha = -\left(k_1 + \frac{\epsilon}{2}\varpi_1^2\right)z_1 - f_3 + m(\hat{\theta}_1 + \beta_1)^T\hat{\Phi}_1 \tag{31}$$

with $k_1, \epsilon > 0$, which yields

$$\dot{z}_1 = -\left(k_1 + \frac{\epsilon}{2}\varpi_1^2\right)z_1 + z_2 + \varpi_1\tilde{x}_1. \tag{32}$$

Step 2. To proceed, compute the time-derivative of z_2 as

$$\begin{aligned}\dot{z}_2 &= g(-\theta_2 x_2 + \bar{u}) + \frac{\partial \Xi}{\partial x_3}[\xi_2 + \xi_1(\hat{x}_1 + \beta_{\hat{x}_1} - \tilde{x}_1)] + \frac{\partial \Xi}{\partial I_{st}}\dot{I}_{st} - \frac{\partial \alpha}{\partial \hat{x}_1}\dot{\hat{x}}_1 \\ &\quad - \frac{\partial \alpha}{\partial x_3}[\xi_2 + \xi_1(\hat{x}_1 + \beta_{\hat{x}_1} - \tilde{x}_1)] - \frac{\partial \alpha}{\partial \hat{\theta}_1}\dot{\hat{\theta}}_1 - \frac{\partial \alpha}{\partial I_{st}}\dot{I}_{st} - \frac{\partial \alpha}{\partial \dot{I}_{st}}\ddot{I}_{st} \\ &= g(-\theta_2 x_2 + \bar{u}) + f_4 - \varpi_2\tilde{x}_1\end{aligned} \tag{33}$$

where $\varpi_2 = \left(\frac{\partial \Xi}{\partial x_3} - \frac{\partial \alpha}{\partial x_3}\right)\xi_1$ and $f_4 = \frac{\partial \Xi}{\partial x_3}[\xi_2 + \xi_1(\hat{x}_1 + \beta_{\hat{x}_1})] - \frac{\partial \alpha}{\partial \hat{x}_1}\dot{\hat{x}}_1 - \frac{\partial \alpha}{\partial x_3}[\xi_2 + \xi_1(\hat{x}_1 + \beta_{\hat{x}_1})] - \frac{\partial \alpha}{\partial \hat{\theta}_1}\dot{\hat{\theta}}_1 + \frac{\partial \Xi}{\partial I_{st}}\dot{I}_{st} - \frac{\partial \alpha}{\partial I_{st}}\dot{I}_{st} - \frac{\partial \alpha}{\partial \dot{I}_{st}}\ddot{I}_{st}$. Design the control law u as

$$\begin{aligned}\bar{u} &= \frac{1}{g}\left[-z_1 - k_2 z_2 - \frac{\epsilon}{2}(\varpi_2^2 + g^2)z_2 + (\hat{\theta}_2 + \beta_2)gx_2 - f_4\right] \\ u &= \frac{1}{c_{13}}\left(\bar{u} + \frac{c_{10}}{x_2}\varphi h\right)\end{aligned} \tag{34}$$

with $k_2 > 0$. Substituting $\bar{u}$ into $\dot{z}_2$ yields

$$\dot{z}_2 = -z_1 - k_2 z_2 - \frac{\epsilon}{2}(\varpi_2^2 + g^2)z_2 + \tilde{\theta}_2 g x_2 - \varpi_2\tilde{x}_1 \tag{35}$$

Now consider the time derivative of the function $V_z = \frac{1}{2}z_1^2 + \frac{1}{2}z_2^2$:

$$\begin{aligned}\dot{V}_z &= -\left(k_1 + \frac{\epsilon}{2}\varpi_1^2\right)z_1^2 + z_1\varpi_1\tilde{x}_1 \\ &\quad - \left(k_2 + \frac{\epsilon}{2}\varpi_2^2 + \frac{\epsilon}{2}g^2\right)z_2^2 + z_2\tilde{\theta}_2 g x_2 - \varpi_2\tilde{x}_1 z_2.\end{aligned} \tag{36}$$

Using the inequalities $\omega_1\tilde{x}_1z_1 \le \frac{1}{2\epsilon}\tilde{x}_1^2 + \frac{\epsilon}{2}\omega_1^2z_1^2$, $-\omega_2\tilde{x}_1z_2 \le \frac{1}{2\epsilon}\tilde{x}_1^2 + \frac{\epsilon}{2}\omega_2^2z_2^2$ and $\tilde{\theta}_2 g z_2 x_2 \le \frac{1}{2\epsilon}\tilde{\theta}_2^2x_2^2 + \frac{\epsilon}{2}g^2z_2^2$, then

$$\dot{V}_z \le -k_1z_1^2 - k_2z_2^2 + \frac{1}{\epsilon}\tilde{x}_1^2 + \frac{1}{2\epsilon}\tilde{\theta}_2^2x_2^2. \tag{37}$$

4.3. Stability Analysis for the Partial-State Feedback Case

The stability analysis of the closed-loop system for the partial-state feedback case is presented in the following theorem.

Theorem 2. *For system (1), it is closed with the adaptive observer (25) and the control laws (31) and (34). Under Assumption 1, it can be guaranteed that all closed-loop signals are bounded and the OER error $y(t) - y_r$ converges to zero as time goes infinity.*

Proof. Choose the following function

$$V_2 = \nu V_{(\tilde{x}_1,\tilde{\theta}_1)} + \frac{1}{2\epsilon\gamma_2}\tilde{\theta}_2^2 + V_z, \quad \nu > 0, \tag{38}$$

whose derivative satisfies, in view of (29) and (37),

$$\begin{aligned}\dot{V}_2 &\le -k_1z_1^2 - k_2z_2^2 - \frac{1}{2\epsilon}x_2^2\tilde{\theta}_2^2 + \left(\frac{1}{\epsilon} - \nu(\Gamma_1\xi_1 + \mu_1)\right)\tilde{x}_1^2 \\ &\le -k_1z_1^2 - k_2z_2^2 - \frac{1}{2\epsilon}x_2^2\tilde{\theta}_2^2 - \tilde{x}_1^2 \le 0\end{aligned} \tag{39}$$

by letting $\nu \ge \dfrac{\epsilon+1}{\epsilon\left(\Gamma_1 \inf\limits_{t\ge0}\xi_1(t) + \mu_1\right)}$. This selection guarantees $\frac{1}{\epsilon} - \nu(\Gamma_1\xi_1 + \mu_1) \le -1$, which upper-bounds the term involving $\tilde{x}_1^2$ by $-\tilde{x}_1^2$. From above we know $V_2(t)$ is bounded and so are signals $z_1(t)$, $z_2(t)$, $\tilde{x}_1(t)$ and $\tilde{\theta}_1(t)$. Similar to the analysis in the proof of Theorem 1, it can be concluded that all closed-loop signals are bounded, and $\lim_{t\to\infty}(z_1(t), \tilde{x}_1(t)) = 0$ by invoking a standard analysis. As a result, it can be concluded from (21) and (22) that $\lim_{t\to\infty} y(t) - y_r = 0$. This completes the proof. □

5. Simulation Results

In this section we present simulation results respectively in the full-state feedback case and the partial-state feedback case for control of the PEMFC air supply system. The physical parameters of model (1) used for simulation is referred to [16]. The evolution of load current used in simulation is shown in Figure 1. Note that, the simulated step load is numerically realized with fast finite slopes so that the derivatives stay bounded, and such sharp transients are used to verify the control performance.

5.1. Full-State Feedback Case

The full-state feedback control scheme in Section 3 is simulated. The controller parameters are set as $k_1 = 50$, $k_2 = 10$, $\epsilon = 1$, $\gamma_1 = \mathrm{diag}\{10^{-9}, 7.5\times10^{-11}, 10^{-4}, 10^{-4}\}$ and $\gamma_2 = 10^{-6}$. The initial values of states are $x_1(0) = 147{,}000$, $x_2(0) = 5400$ and $x_3(0) = 157{,}000$. The initial values of adaptive laws are $\hat{\theta}_1(0) = [37, 30, 100{,}000, 300]^T$ and $\hat{\theta}_2(0) = 6$. For comparison, the Lyapunov-based adaptive dynamic surface controller is also tested here. Specifically, it takes the following form,

$$\begin{aligned} \alpha &= -k_1 z_1 + m\hat{\theta}_1^T \Phi_1 - f_1 \\ \bar{u} &= \frac{1}{g}\left[-z_1 - k_2 z_2 + \hat{\theta}_2 g x_2 - f_2\right] \\ u &= \frac{1}{c_{13}}\left(\bar{u} + \frac{c_{10}}{x_2}\varphi h\right) \end{aligned} \tag{40}$$

where $z_1 = y - y_r$, $z_2 = \Xi - \alpha_c$, $f_2 = \frac{\partial \Xi}{\partial x_3}\dot{x}_3 + \frac{\partial \Xi}{\partial I_{st}}\dot{I}_{st} - \dot{\alpha}_c$ with $\dot{\alpha}_c = -\tau_c(\alpha_c - \alpha)$ being a low-pass filter, $\tau_c > 0$ and k_1 and k_2 are same parameters in the proposed controller. The adaptive laws $\hat{\theta}_1, \hat{\theta}_2$ are designed as

$$\begin{aligned} \dot{\hat{\theta}}_1 &= -\bar{\gamma}_1 \Phi_1 z_1 \\ \dot{\hat{\theta}}_2 &= -\bar{\gamma}_2 x_2 z_2 \end{aligned} \tag{41}$$

which is based on the idea of Lyapunov cancellation with $\bar{\gamma}_1 \in \mathbb{R}^{4\times 4} > 0$ and $\bar{\gamma}_2 > 0$.

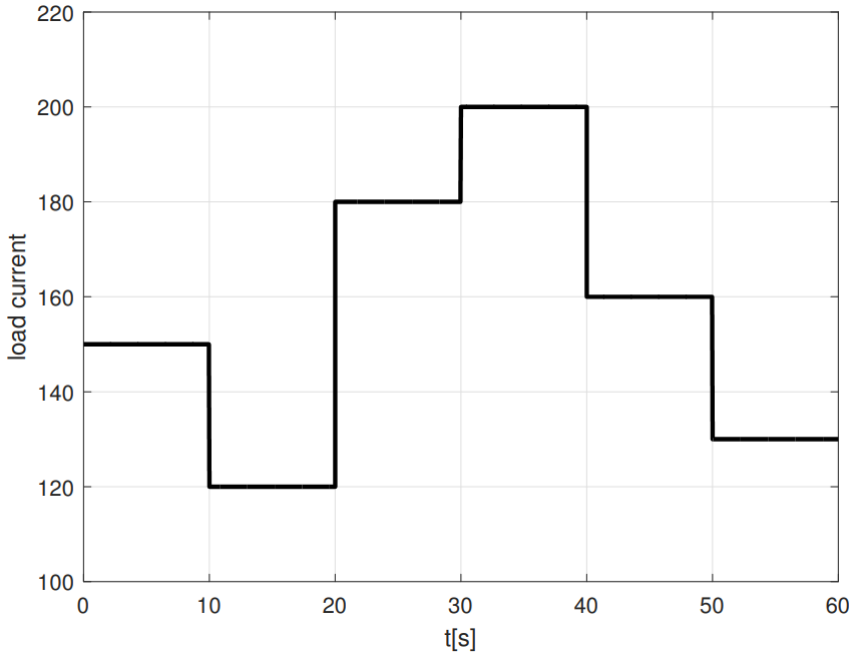


Figure 1. Evolution of load current.

To guarantee fair comparison, several principles are followed when configuring the Lyapunov-based benchmark controller. First, the backstepping control gains k_1 and k_2 are kept identical to those used in the proposed I&I adaptive scheme. Second, both controllers are tested under the same system model, load profile, initial state values, and noise disturbances. Third, the adaptive gains and low-pass filter parameter of the Lyapunov-based controller are carefully tuned to attain its best achievable performance. Specifically, besides common control parameters k_1 and k_2 which are set as the same with the proposed scheme, the adaptation gains $\bar{\gamma}_1$ and $\bar{\gamma}_2$ are set as $\bar{\gamma}_1 = \text{diag}\{10^{-4}, 10^{-4}, 1, 1\}$ and $\bar{\gamma}_2 = 10^{-4}$, and $\tau_c = 100$.

In the parameter-variation test, the true physical plant parameters μ_1, μ_2, μ_3, μ_4 and c_9 are subjected to -20% step changes at $t = 25$ s. These are runtime variations of actual model parameters inside the simulation plant. Note that such plant-parameter changes should be distinguished from initial parameter estimation errors: the adaptive estimates $\hat{\theta}_1(0)$ and $\hat{\theta}_2(0)$ are initialized away from nominal true values, which generates initial estimation error at the start of simulation. The same initial estimation errors are adopted for both the proposed I&I controller and Lyapunov-based benchmark. Moreover, the control input is saturated within $[0, 600]$ to mimic practical actuator saturation.

Numerical simulations are conducted to verify the effectiveness of the proposed scheme, with the Lyapunov-based scheme adopted as the baseline for comparison. Figure 2 presents the time evolution of the OER regulation error for both control strategies. In the initial phase (0–4 s) and two transient phases in (23–34 s) of parameter change and load variation respectively, although instantaneous error peaks can be comparable at certain load-switching moments, the tracking error of the proposed scheme decays more rapidly after each transient. Figure 3 illustrates the trajectories of the control input (compressor motor voltage). The proposed controller generates smoother control signals with lower peak values, avoiding excessive voltage fluctuations that may damage the compressor. In contrast, the Lyapunov-based controller produces larger and more oscillatory control inputs, indicating potential mechanical stress. To test the robustness against process disturbances, a uniformly distributed random signal is additively injected into the dynamics of each state, taking values uniformly over $[-10^4, 10^4]$. The same disturbance signal is used for both the proposed I&I controller and the Lyapunov-based benchmark to ensure comparison fairness. As shown in Figure 4, the proposed method maintains stable OER regulation with smaller error fluctuations, while the Lyapunov-based method suffers from more significant error deviations. This confirms that the I&I adaptive framework enhances the system's robustness against external disturbances and unmodeled dynamics.

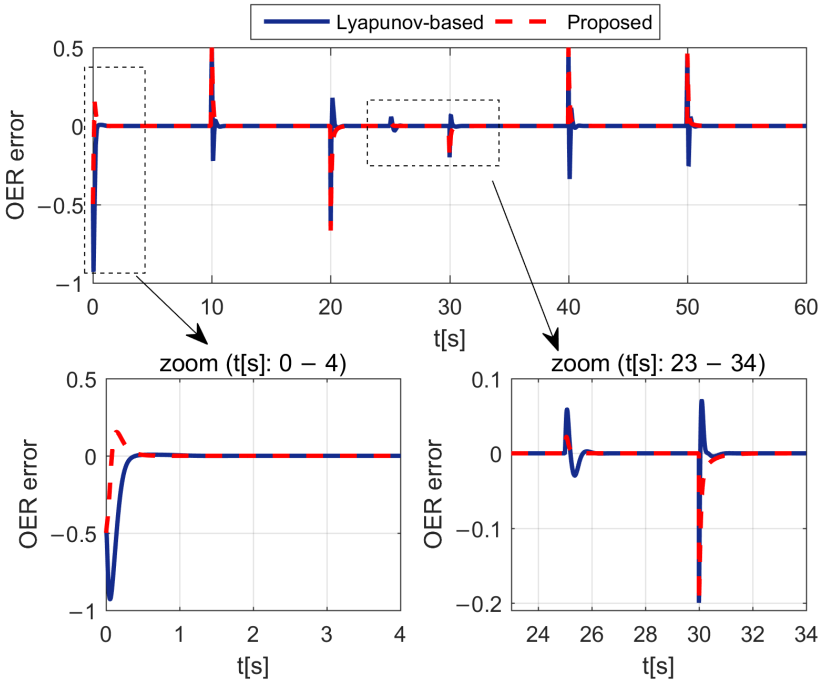


Figure 2. Case 1: Evolution of OER regulation errors.

To quantitatively compare the control performance under disturbance, three metrics, including integral of absolute error (IAE), integral of squared error (ISE), and peak control magnitude (U_{peak}), are calculated and listed in Table 1. It can be seen that the proposed I&I adaptive controller achieves lower IAE and ISE than the Lyapunov-based adaptive controller, which quantitatively confirms the improved OER regulation accuracy. Moreover, the peak value of control input is significantly reduced for the proposed scheme, while the Lyapunov-based scheme reaches the upper level of the control saturation, which indicates milder control effort and less mechanical stress on the air compressor of the proposed scheme.

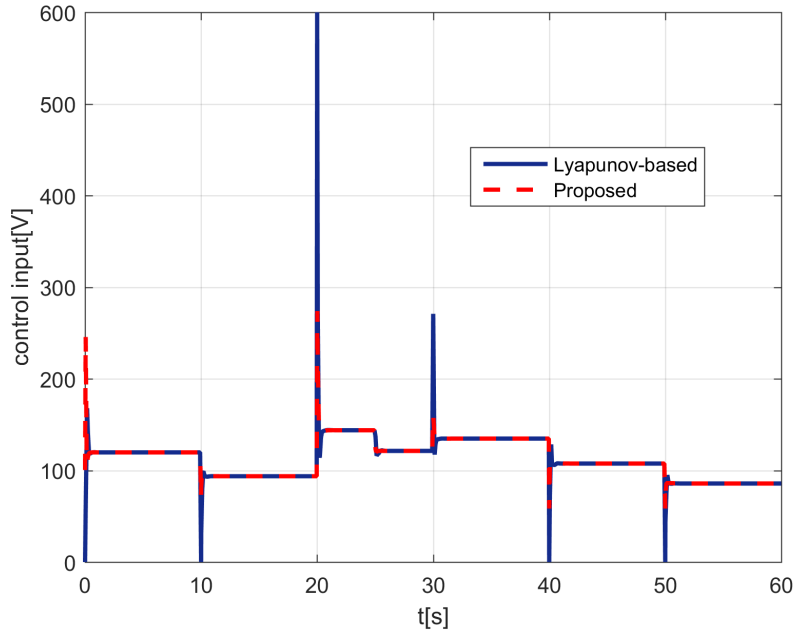


Figure 3. Case 1: Evolution of control inputs.

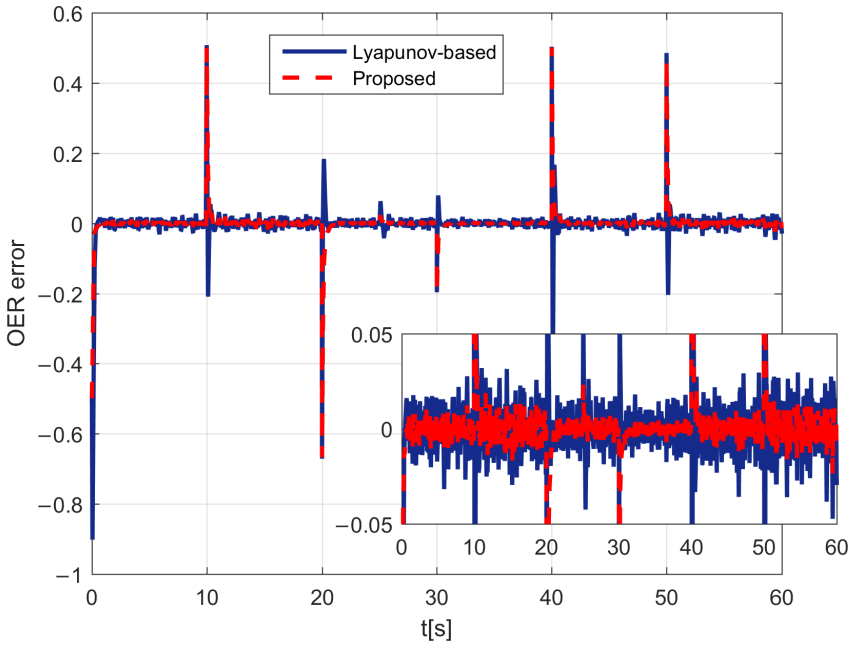


Figure 4. Case 1: Evolution of OER regulation errors under unmodeled noises.

Table 1. Quantitative performance indices for full-state feedback case with disturbance.

Index	Proposed I&I	Lyapunov-Based Adaptive
IAE	0.49	0.82
ISE	0.080	0.15
U_{peak}	274.03	600.00

5.2. Partial-State Feedback Case

The partial-state feedback control scheme in Section 4 is simulated here. The controller parameters are set as $k_1 = 50$, $k_2 = 10$, $\epsilon = 1$, $\Gamma_1 = 1$, $\gamma_1 = \text{diag}\{3 \times 10^{-9}, 3 \times 10^{-9}, 10^{-5}, 10^{-5}\}$

and $\gamma_2 = 10^{-6}$. For comparison, the ESO technique [25] is used to recover the unknown state x_1 in scheme (40) and (41). Specifically, the ESO is constructed as

$$\dot{\hat{x}}_3 = \phi h - \phi c_{16} x_3 + \hat{\vartheta} + l_1 \cdot (x_3 - \hat{x}_3)$$
$$\dot{\hat{\vartheta}} = l_2 \cdot (x_3 - \hat{x}_3)$$

where $l_1 = 2\omega$ and $l_2 = \omega^2$ are the observer gains with $\omega > 0$, and the state $\hat{\vartheta}$ is used to replace the original state x_1 in (40) and (41) through the following relationship

$$\hat{x}_1 = \frac{\hat{\vartheta}}{c_{16}\phi}.$$

The bandwidth parameter of ESO is also properly adjusted for satisfactory state reconstruction. In simulation the parameter ω is set as $\omega = 50$, and the other parameters are set the same as in the previous case.

In simulation results for this case, the true physical plant parameters μ_1, μ_2, μ_3, μ_4 and c_9 are also subjected to -20% step changes at $t = 25$ s. The results are shown in Figures 5–8. Figure 5 shows the OER regulation error curves. Comparable instantaneous error peaks can be observed at several load-switching moments; nevertheless, the error trajectory of the proposed scheme exhibits weaker oscillation after initial transient stage and each load transient, together with superior integral tracking performance under load transients and parameter variations (see Table 2). As depicted in Figure 6, the control input of the proposed method generates more stable control signals with reduced chattering and peak voltage, which mitigates mechanical stress on the air compressor. This is attributed to the unified design of adaptive observer and backstepping control, which avoids the decoupled design defects of traditional ESO-based methods. In Figure 7, the observation error of the unmeasurable cathode pressure of the proposed adaptive observer method has significantly smaller magnitudes during load transients. Under the same unmodeled noise disturbances as in Section 5.1, the proposed controller still maintains tight OER regulation as shown in Figure 8, while the ESO & Lyapunov-based method exhibits larger error oscillations. This demonstrates that the I&I adaptive framework provides better robustness for partial-state feedback systems with parametric uncertainties and unmeasurable states.

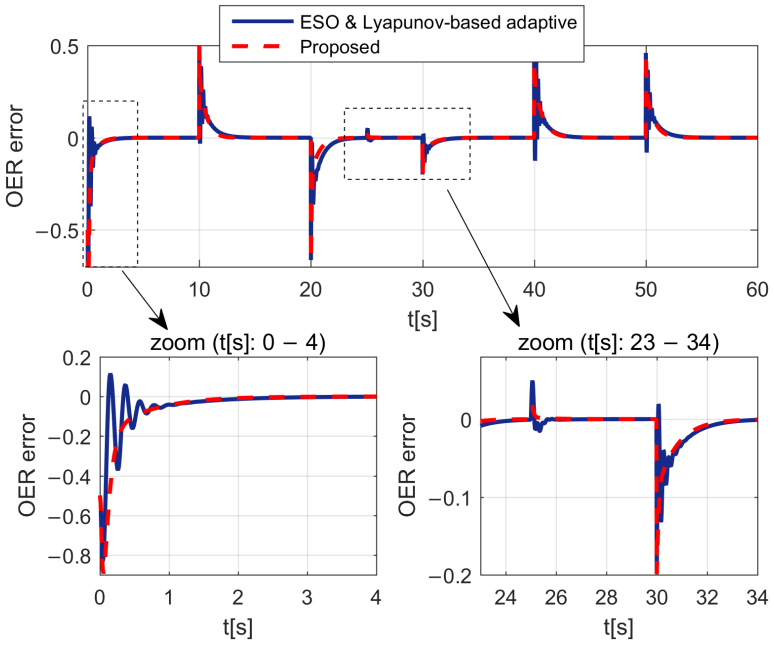


Figure 5. Case 2: Evolution of OER regulation errors.

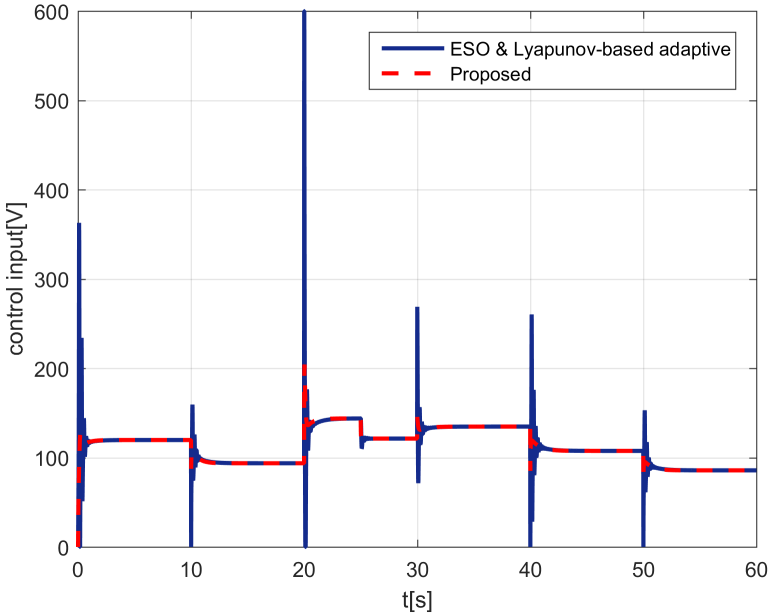


Figure 6. Case 2: Evolution of control inputs.

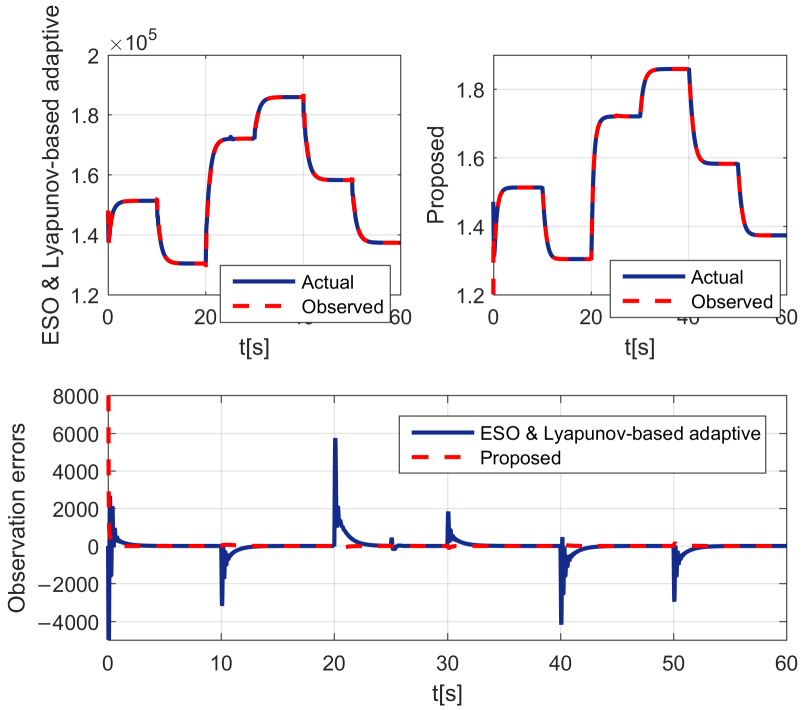


Figure 7. Case 2: Evolution of state observation errors of x_1.

The quantitative performance indices for the partial-state feedback scenario with disturbance are reported in Table 2. Compared with the ESO-plus-Lyapunov-based adaptive strategy, the developed unified I&I adaptive observer-backstepping scheme yields smaller IAE and ISE indices as well as reduced peak control voltage, demonstrating its superiority in both transient regulation performance and actuator protection. Moreover, to quantitatively assess observer performance, the integral of absolute observation error $\mathrm{IAE}_{\mathrm{obs}}$ and integral of squared observation error $\mathrm{ISE}_{\mathrm{obs}}$ for $\tilde{x}_1(t)$ are computed and summarized in Table 2. Compared with the ESO-based observer, the proposed I&I adaptive observer yields lower $\mathrm{IAE}_{\mathrm{obs}}$ and $\mathrm{ISE}_{\mathrm{obs}}$, which quantitatively confirms its better state-reconstruction accuracy for the unmeasurable cathode pressure.

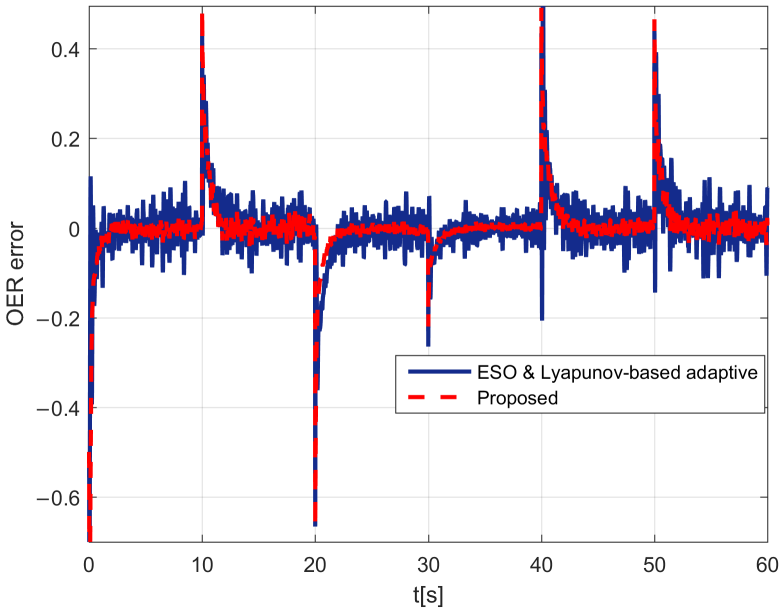


Figure 8. Case 2: Evolution of OER regulation errors under unmodeled noises.

Table 2. Quantitative performance indices for partial-state feedback case with disturbance.

Index	Proposed I&I	ESO + Lyapunov-Based Adaptive
IAE	1.49	2.28
ISE	0.26	0.27
U_{peak}	212.15	600.00
IAE_{obs}	3.04×10^3	1.67×10^4
ISE_{obs}	1.56×10^7	1.62×10^7

5.3. Practical Implementation Considerations

This section discusses practical issues for deploying the proposed I&I adaptive control scheme on PEMFC air supply systems. The partial-state feedback framework only requires the measurement of the compressor control voltage and the state x_3, while the cathode pressure x_1 is reconstructed via the I&I observer, removing the need for an additional in-channel cathode pressure sensor.

For real-time embedded implementation, the continuous-time observer and control laws should be discretized with a fixed sampling period matching the dynamic bandwidth of the air supply system. The adaptive parameter update law is executed synchronously at each sampling instant. The control signal is bounded by the hardware voltage limit of the air compressor; anti-windup strategies can be further incorporated if actuator saturation occurs frequently in real operation.

Moreover, the proposed algorithm mainly consists of algebraic calculations and recursive adaptive updates, leading to modest computational burden compatible with low-cost microcontrollers widely adopted in fuel-cell systems. Experimental validation on a PEMFC test bench will be conducted in our future research.

6. Conclusions

This paper has presented an I&I adaptive backstepping control framework for the air supply system of a PEMFC operating under unmeasurable state conditions. To accommodate uncertainties, an I&I adaptive full-state feedback controller was first developed, which guarantees asymptotic regulation of the OER while preserving satisfactory transient charac-

teristics. Recognizing the practical inaccessibility of cathode pressure measurements, an I&I adaptive observer-based partial-state feedback strategy was further proposed, wherein both unknown parameters and unmeasured states are estimated within a unified design framework. Closed-loop stability of both proposed schemes was rigorously established via Lyapunov analysis, and the effectiveness of the control strategies was corroborated through numerical simulations conducted under parametric variations. The results demonstrate that the proposed I&I-based methodology offers a promising and theoretically sound solution for robust OER regulation in PEMFC air supply systems. Future work will focus on experimental validation and the extension of the proposed framework to full parameter estimation and fault-tolerant operation.

Author Contributions: Conceptualization, Q.H., X.Z., S.X., Z.L. and M.F.; methodology, Q.H.; software, Q.H.; validation, Q.H., X.Z., S.X., Z.L. and M.F.; formal analysis, Q.H.; investigation, Q.H.; writing—original draft preparation, Q.H.; writing—review and editing, Q.H., X.Z., S.X., Z.L. and M.F.; visualization, Q.H.; supervision, X.Z., S.X., Z.L. and M.F.; project administration, X.Z.; funding acquisition, X.Z. All authors have read and agreed to the published version of the manuscript.

Funding: This work has been supported by the Key R&D Program of the Ministry of Science and Technology (Grant No. 2023YFB3209805), and the Zhejiang Provincial Key R&D Project (Grant No. 2025C01146).

Data Availability Statement: Data are contained within the article.

Conflicts of Interest: Mingyou Fu is employed by Beijing Zhuoyi Intelligent Technology Co., Ltd. The remaining authors declare that the research was conducted in the absence of any commercial or financial relationships that could be construed as a potential conflict of interest. The authors declare that this study received funding from the Key R&D Program of the Ministry of Science and Technology and the Zhejiang Provincial Key R&D Project. The funder was not involved in the study design; collection, analysis, or interpretation of data; the writing of this article; or the decision to submit it for publication.

References

1. Daud, W.; Rosli, R.; Majlan, E.; Hamid, S.; Mohamed, R.; Husaini, T. PEM fuel cell system control: A review. *Renew. Energy* **2017**, *113*, 620–638. [CrossRef]
2. Wang, Y.; Wang, Y.; Xu, J.; Chai, T. Observer-based discrete adaptive neural network control for automotive PEMFC air-feed subsystem. *IEEE Trans. Veh. Technol.* **2021**, *70*, 3149–3163. [CrossRef]
3. Chen, J.H.; He, P.; Cai, S.J.; He, Z.H.; Zhu, H.N.; Yu, Z.Y.; Yang, L.Z.; Tao, W.Q. Modeling and temperature control of a water-cooled PEMFC system using intelligent algorithms. *Appl. Energy* **2024**, *372*, 123790. [CrossRef]
4. Xu, H.; Wang, L.; Liu, Z.; Su, H.; Ortega, R. Online identification of pemfc polarization curves with nonlinear concentration loss. *IEEE Trans. Ind. Electron.* **2025**, *72*, 7544–7552. [CrossRef]
5. Xu, H.; Yang, Y.; Wu, Z.G.; Su, H.; Wang, L. Hierarchical optimal temperature regulation for PEMFCs via generalized data-enabled predictive control. *IEEE Trans. Ind. Electron.* **2026**, *73*, 3083–3092. [CrossRef]
6. Li, Q.; Yin, L.; Yang, H.; Wang, T.; Qiu, Y.; Chen, W. Multiobjective optimization and data-driven constraint adaptive predictive control for efficient and stable operation of PEMFC system. *IEEE Trans. Ind. Electron.* **2021**, *68*, 12418–12429. [CrossRef]
7. Wang, Y.; Wang, Y.; Wang, D.; Chai, T. Observer-based composite adaptive type-2 fuzzy control for PEMFC air supply systems. *IEEE Trans. Fuzzy Syst.* **2022**, *30*, 515–529. [CrossRef]
8. Talj, R.J.; Hissel, D.; Ortega, R.; Becherif, M.; Hilairet, M. Experimental validation of a PEM fuel-cell reduced-order model and a moto-compressor higher order sliding-mode control. *IEEE Trans. Ind. Electron.* **2009**, *57*, 1906–1913. [CrossRef]
9. Garcia-Gabin, W.; Dorado, F.; Bordons, C. Real-time implementation of a sliding mode controller for air supply on a PEM fuel cell. *J. Process Control* **2010**, *20*, 325–336. [CrossRef]
10. Liu, J.; Gao, Y.; Su, X.; Wack, M.; Wu, L. Disturbance-observer-based control for air management of PEM fuel cell systems via sliding mode technique. *IEEE Trans. Control Syst. Technol.* **2018**, *27*, 1129–1138. [CrossRef]
11. Souissi, A. Adaptive sliding mode control of a PEM fuel cell system based on the super twisting algorithm. *Energy Rep.* **2021**, *7*, 3390–3399. [CrossRef]

12. Abbaker, A.M.O.; Wang, H.; Tian, Y. Adaptive integral type-terminal sliding mode control for PEMFC air supply system using time delay estimation algorithm. *Asian J. Control* **2022**, *24*, 217–226. [CrossRef]
13. Zhang, J.; Liu, G.; Yu, W.; Ouyang, M. Adaptive control of the airflow of a PEM fuel cell system. *J. Power Sources* **2008**, *179*, 649–659. [CrossRef]
14. Li, P.; Chen, J.; Cai, T.; Zhang, B. Adaptive control of air delivery system for PEM fuel cell using backstepping. In *Proceedings of the 2011 8th Asian Control Conference (ASCC), Kaohsiung, Taiwan, China, 15–18 May 2011*; IEEE: New York, NY, USA, 2011; pp. 1282–1287.
15. Guo, X.; Fan, N.; Dong, Z.; Wang, C. Adaptive prescribed performance control for PEM fuel cell air supply systems with unknown air compressor faults. *IEEE Trans. Ind. Electron.* **2024**, *71*, 7664–7672. [CrossRef]
16. Meng, J.; Guo, Q.; Yue, M.; Diallo, D. A Lyapunov-based adaptive control strategy with fault-tolerant objectives for proton exchange membrane fuel cell air supply systems. *Appl. Energy* **2024**, *376*, 124275. [CrossRef]
17. Fan, N.; Guo, X.; Wang, C.; Dong, Z.; Liu, L.; Yang, J. Adaptive coordinated control for nonlinear PEM fuel cell air supply systems. *IEEE Trans. Ind. Electron.* **2025**, *72*, 5312–5321. [CrossRef]
18. Li, Y.; Fan, Y.; Li, K.; Liu, W.; Tong, S. Adaptive optimized backstepping control-based RL algorithm for stochastic nonlinear systems with state constraints and its application. *IEEE Trans. Cybern.* **2021**, *52*, 10542–10555. [CrossRef]
19. Wang, Z.; Guo, X.; Dong, Z.; Fan, N.; Cao, S. Fixed time adaptive fault tolerant sliding mode control of PEMFC air supply system. *Int. J. Hydrogen Energy* **2024**, *55*, 1434–1444. [CrossRef]
20. Du Phan, V.; Trinh, H.A.; Ahn, K.K. Adaptive disturbance observer-based terminal sliding mode algorithm for a mini excavator proton exchange membrane fuel cell air feeding system. *Appl. Energy* **2025**, *382*, 125304. [CrossRef]
21. Xiong, W.; Zeng, X.; Zeng, X.; Liu, T. A fuzzy adaptive sliding-mode control method with improved ESO for a PEMFC air supply system. *Int. J. Hydrogen Energy* **2025**, *128*, 395–405. [CrossRef]
22. Astolfi, A.; Karagiannis, D.; Ortega, R. *Nonlinear and Adaptive Control with Applications*; Springer: London, UK, 2008. [CrossRef]
23. Talj, R.; Ortega, R.; Astolfi, A. Passivity and robust PI control of the air supply system of a PEM fuel cell model. *Automatica* **2011**, *47*, 2554–2561. [CrossRef]
24. Yuan, H.; Dai, H.; Wei, X.; Ming, P. Model-based observers for internal states estimation and control of proton exchange membrane fuel cell system: A review. *J. Power Sources* **2020**, *468*, 228376. [CrossRef]
25. Meng, J.; Guo, Q.; Zhang, X.; Lin, J.; Yue, M. A robust adaptive control strategy for oxygen excess ratio regulation in fuel cell systems with reduced control effort. *ISA Trans.* **2025**, *167*, 1495–1505. [CrossRef]
26. Baroud, Z.; Benmiloud, M.; Benalia, A.; Ocampo-Martinez, C. Novel hybrid fuzzy-PID control scheme for air supply in PEM fuel-cell-based systems. *Int. J. Hydrogen Energy* **2017**, *42*, 10435–10447. [CrossRef]
27. Talj, R.; Ortega, R.; Hilairet, M. A controller tuning methodology for the air supply system of a PEM fuel-cell system with guaranteed stability properties. *Int. J. Control* **2009**, *82*, 1706–1719. [CrossRef]
28. Kim, B.M.; Yoo, S.J. Decentralized event-triggered adaptive control for interconnected nonlinear dynamics of constrained air supply and thermal management systems of PEMFCs. *Nonlinear Dyn.* **2021**, *103*, 791–808. [CrossRef]

Disclaimer/Publisher's Note: The statements, opinions and data contained in all publications are solely those of the individual author(s) and contributor(s) and not of MDPI and/or the editor(s). MDPI and/or the editor(s) disclaim responsibility for any injury to people or property resulting from any ideas, methods, instructions or products referred to in the content.